RESEARCH ARTICLE

QCTP: A Novel Pre-Coding Approach for PAPR Reduction in IM/DD Systems

IDRIS CINEMRE [1], (Member, IEEE), **GOKCE HACIOGLU** [2],
AND TOKTAM MAHMOODI [1], (Senior Member, IEEE)
[1] Department of Engineering, Faculty of Natural, Mathematical and Engineering Sciences, King's College London, WC2R 2LS London, U.K.
[2] Electrical and Electronics Engineering Department, Karadeniz Technical University, 61080 Trabzon, Türkiye

Corresponding author: Idris Cinemre (idris.1.cinemre@kcl.ac.uk)

ABSTRACT Orthogonal frequency division multiplexing (OFDM) is critical for high-speed visible light communication (VLC) transmission; however, it suffers from a high peak-to-average power ratio (PAPR) problem. Among PAPR reduction techniques, pre-coding methods have shown promising advantages such as signal independence and no requirement for signaling overhead. This paper introduces a novel pre-coding technique termed quartered composite transform pre-coding (QCTP), which employs four newly developed orthogonal pre-coding matrices applied to four equally divided segments of modulated data, thereby enhancing the PAPR performance of VLC systems utilizing OFDM. This methodology allows the utilization of a single-tap equalizer, achieving over a 6 dB reduction in PAPR compared to conventional DCT pre-coding and surpassing the PAPR performance of DCT-hybridized (DCT & μ-compounding and DCT & Gaussian matrix) pre-coding techniques. This enhancement is accomplished without compromising bit error rate (BER) performance, all while maintaining reduced complexity.

INDEX TERMS PAPR, OFDM, VLC, DCT, DST.

I. INTRODUCTION

Visible light communication (VLC) is a sophisticated optical wireless communication method that leverages visible light emitted by commercial-off-the-shelf light-emitting diode (LED) sources to transmit data over short distances, modulated by intensity modulation (IM) in a way that satisfies lighting requirements and captured by a photodiode on the receiver end via direct detection (DD). A notable challenge in achieving high data rates via VLC lies in effectively exploiting the limited spectral bandwidth of white LEDs [1], [2], [3]. It is highlighted in the literature that implementing orthogonal frequency division multiplexing (OFDM) as a modulation technique characterized by its high spectral efficiency can offer a viable solution to this challenge. Moreover, OFDM is a compelling choice for high-speed data transmission in VLC, owing to its resilience against inter-symbol interference (ISI), improved optical power

efficiency, and adaptability to diverse channel conditions, requiring just a simple single-tap equalizer at the receiver [4]. Conventional OFDM, based on fast Fourier transform (FFT), generates bipolar and complex symbols unsuitable for VLC, requiring real and unipolar symbols. Hermitian symmetry is employed in OFDM structure to produce real-valued symbols, and the two most widespread techniques have been reported to ensure unipolar and positive symbols: Direct current biased optical OFDM (DCO-OFDM) [5], [6], [7], adding positive DC bias, and asymmetrically clipped optical OFDM (ACO-OFDM) [8], [9], [10], clipping negative symbols at zero.

A notable drawback of utilizing OFDM in wireless communication is having a high peak-to-average power ratio (PAPR), which arises from the superposition of several distinct orthogonal subcarriers [11], [12], [13]. In VLC, a high PAPR can cause the LED to operate beyond its designed power levels (i.e in a nonlinear zone), resulting in energy inefficiency, a shorter lifespan of LED, and signal distortion in the transmitted signal which leads to a worsened

The associate editor coordinating the review of this manuscript and approving it for publication was Yunlong Cai [ID].

bit error rate (BER) [14]. Therefore, PAPR reduction methods are essential for VLC systems to retain signal quality and enhance energy efficiency.

The PAPR reduction strategies for optical OFDM have been thoroughly investigated, which may be broadly classified into three distinct classes; multiple signalling techniques, signal distortion-based methods, and pre-coding schemes [15]. In multiple signalling approaches, several candidate signals with identical information are generated, and the one with the lowest PAPR is selected for transmission. Selective mapping (SLM) [16], [17], partial transmit sequence (PTS) [18], [19], [20], pilot-assisted (PA) [7], [21], [22], and tone reservation (TR) [23], [24], [25] can be listed as the common methods. These methods typically necessitate supplementary information alongside the actual data, leading to decreased bandwidth efficiency and increased computational complexity.

The methods based on signal distortion reduce the PAPR by employing techniques such as clipping high signal peaks [26], [27], [28], compressing large peaks utilizing non-linear companding [29], [30], and stretching the constellation [31]. Although these solutions are straightforward to implement, they introduce distortion noises that can adversely affect the performance of the system. It should be noted that multiple signalling approaches are frequency domain techniques, whereas distortion methods are time domain techniques applied after the inverse FFT (IFFT) to reduce PAPR.

The pre-coding PAPR reduction schemes are also implemented in the frequency domain with lower complexity than multiple signalling techniques. In this approach, the modulated data is multiplied by a pre-coding matrix at the transmitter before the IFFT block in the OFDM structure, and the inverse pre-coding matrix is applied at the receiver after the FFT block to recover the modulated data. Various transforms have been employed as pre-coding matrices to reduce PAPR, including discrete cosine transform (DCT) [32], zadoff-chu transform (ZCT) [33], discrete Fourier transform (DFT) [34], [35], walsh-hadamard transform (WHT) [36], discrete hartley transform (DHT) [37], [38], and vandermonde-like matrix (VLM) transform [13]. Pre-coding has a number of advantages over other approaches, including signal independence, no requirement for signalling overhead, and no significant degradation in BER performance.

The inherent energy compaction property of the DCT renders it an appealing technique for pre-coding, as this feature has been successfully employed in various signal processing applications, including image processing and video compression [39]. The literature contains several attempts to further enhance PAPR by combining DCT-precoding with other methods. For instance, the article [40] proposes a hybrid PAPR reduction system for DCO-OFDM, which involves the application of DCT pre-coding, followed by multiplication of the IFFT output with a Gaussian matrix to reduce PAPR. This combined method achieves a modest PAPR improvement of approximately 1 dB without compromising

BER performance when compared to the DCT pre-coded method. In [36], the DCT pre-coding scheme is integrated with the clipping method to decrease PAPR for DCO-OFDM, yielding an enhancement of approximately 2 dB.

The study outlined in [41] simultaneously applies multiple DCT pre-coding techniques to an IM/DD system by grouping subcarriers. The utilization of groups of two results in a 15% reduction in complexity but leads to around 1 dB increase in PAPR and degraded BER performance. In [42], to minimise PAPR in DCO-OFDM, the paper recommends combining DCT precoding with two distinct companding approaches (specifically, μ-law and A-law). The study reveals around a 3 dB decrease in PAPR for both methods without a loss in BER performance.

This paper introduces a novel pre-coding method that involves partitioning the modulated data into four equal subsets and utilizing innovative orthogonal quartered composite transform pre-coding (QCTP) matrices prior to the IFFT transformation, while also incorporating the approach defined in [43]. The QCTP method offers all the advantages of pre-coding PAPR reduction techniques, ensuring efficient PAPR reduction without sacrificing BER performance, and achieves these benefits with reduced complexity. The remainder of this paper is organized as follows: Section II presents the system model of conventional DCO-OFDM, DCT pre-coded DCO-OFDM, and the proposed QCTP method applied to DCO-OFDM; Section III outlines the simulation environment, detailing the model room and channel response of a typical indoor setting, along with the comparative analysis of BER, PAPR, and computational complexity; finally, Section IV offers concluding remarks and discusses future directions.

Notations: The bold small letters are denoted as vectors and bold uppercase letters to refer to matrices. $[\cdot]^T$ represents the transpose of a vector or a matrix, z^* indicates the complex conjugate of z, $\mathbf{I}$ is $N \times N$ identity matrix, and $\mathbf{0}$ is N-length zero vector.

II. SYSTEM MODEL
A. CONVENTIONAL DCO-OFDM
In DCO-OFDM, data are first mapped into complex-valued symbols,

$$\mathbf{s} = \left[s_0, s_1, \ldots, s_{(\frac{N}{2}-2)} \right]^T \in \mathbb{C}^{(\frac{N}{2}-1)}, \quad (1)$$

employing a modulation scheme (e.g. QAM) as shown in Fig. 1(a). Then, these symbols are stored in $\mathbf{x} \in \mathbb{C}^N$ which must exhibit Hermitian symmetry, depicted as

$$\mathbf{x} = \left[0, s_0, s_1, \ldots, s_{(\frac{N}{2}-2)}, 0, s^*_{(\frac{N}{2}-2)}, \ldots, s^*_1, s^*_0 \right]^T, \quad (2)$$

to ensure a real-valued output, $\mathbf{x}_f \in \mathbb{R}^N$, after the execution of IFFT, $\mathbf{F}^H \in \mathbb{C}^{N \times N}$,

$$\mathbf{x}_f = \mathbf{F}^H \mathbf{x}. \quad (3)$$

The IFFT matrix, denoted as $\mathbf{F}^H$, is defined as $\left(\mathbf{F}^T \right)^*$, where
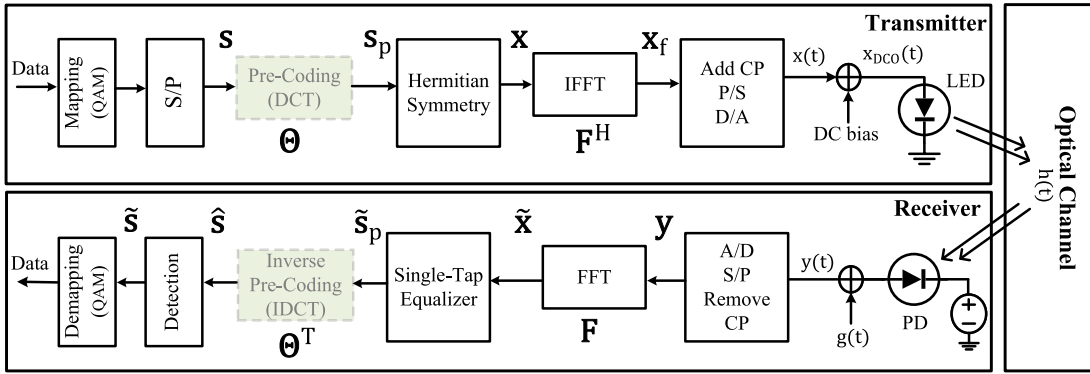
FIGURE 1. Block diagram of (a) conventional DCO-OFDM (without green boxes) and (b) DCT pre-coded DCO-OFDM (with green boxes).

the FFT matrix is given as $\mathbf{F} = (f_{k,l})_{0 \le k, l \le N-1}$, with each element of $\mathbf{F} \in \mathbb{C}^{N \times N}$ represented as

$$f_{k,l} = \left(\frac{1}{\sqrt{N}} \right) e^{-j \frac{2\pi kl}{N}}. \tag{4}$$

It is assumed that the cyclic prefix (CP) with the length of being set to no less than the tap number of the channel impulse response (CIR) is appended prior to transmission. A ϑ-tap CIR is denoted as

$$\mathbf{h} = [h_0, h_1, h_2, \ldots, h_{\vartheta-1}]. \tag{5}$$

The samples are subsequently formed into a serial sequence and sent to a digital-to-analog (D/A) converter. In DCO-OFDM, a DC bias is then added to the converted electrical signal to eliminate the bipolar nature of the signal and make IM/DD feasible. Note that any remaining negative peaks are required to be clipped before driving the LED to convert this electrical signal into an optical signal.

After passing through the optical channel, the transmitted visible light signal is captured by a photodetector (PD) and subsequently converted to an analog electrical signal at the receiver; then, an analog-to-digital converter (A/D) is used to convert the signal to digital, the cyclic prefix (CP) is removed from the samples, and the data is transformed from serial to parallel (S/P). The system operates under the assumption that the channel response is accurately characterized with the ϑ-taps. The received N samples are denoted by $\mathbf{y} \in \mathbb{R}^N$ as

$$\mathbf{y} = \mathbf{C}\mathbf{x}_f + \mathbf{g} \tag{6}$$

where $\mathbf{C} \in \mathbb{R}^{N \times N}$ is the circulant channel matrix created utilizing (5) as defined in [44] and $\mathbf{g} \in \mathbb{R}^N \sim \mathcal{N}(\mathbf{0}, \sigma_g^2 \mathbf{I})$ stands for additive white Gaussian noise (AWGN), that models the thermal and shot noise. The elements of $\tilde{\mathbf{x}} \in \mathbb{C}^N$ can be estimated by applying N-point FFT, $\mathbf{F} \in \mathbb{C}^{N \times N}$,

$$\tilde{\mathbf{x}} = \mathbf{F}\mathbf{y} = \Lambda \mathbf{x} + \mathbf{F}\mathbf{g}, \tag{7}$$

where $\Lambda \in \mathbb{C}^{N \times N}$ is diagonal matrix given as

$$\Lambda = \mathbf{F}\mathbf{C}\mathbf{F}^H. \tag{8}$$

Unbiased estimations of $\mathbf{s}$, positioned within $\mathbf{x}$ as shown in (2), are denoted as $\tilde{\mathbf{s}}$. The nth elements of $\tilde{\mathbf{s}}$ is calculated as

$$\tilde{s}_n = \frac{\tilde{x}_{n+1}}{\Lambda_{n+1,n+1}}, \tag{9}$$

where $n = 0, 1, 2, \ldots, (\frac{N}{2} - 2)$. The estimation of the transmitted $\frac{N}{2} - 1$ symbols is stored in the $\tilde{\mathbf{s}}$ array. The receiver makes the decision about n^{th} transmitted symbol s_n by using the maximum likelihood decision (MLD) rule as

$$\hat{s}_n = arg \min_{p_i} (|\tilde{s}_n - p_i|^2) \tag{10}$$

where p_i denotes one of the P constellation points (i.e. $i = 0, 1, \ldots, P - 1$) and $\hat{s}_n$ denotes n^{th} element of the detected symbols. Finally, these symbols are demapped into data.

B. DCT PRE-CODED DCO-OFDM

On the transmitter side, the pre-coding is employed prior to storing mapped symbols, $\mathbf{s} \in \mathbb{C}^{(\frac{N}{2}-1)}$, into $\mathbf{x}$ as in (2) as shown in Fig. 1(b). The DCT pre-coding matrix is defined as $\Theta = (\theta_{k,l})_{0 \le k, l \le N-1}$ where $\theta_{k,l}$ is the $(k, l)^{th}$ element of $\Theta \in \mathbb{R}^{N \times N}$ and given as

$$\theta_{k,l} = \begin{cases} \sqrt{\dfrac{1}{N}}, & k = 0 \\ \sqrt{\dfrac{1}{N}} \cos \left[\dfrac{\pi (2l+1) k}{2N} \right], & k = 1, \ldots, N-1. \end{cases} \tag{11}$$

The pre-coded symbols, $\mathbf{s}_p \in \mathbb{C}^{(\frac{N}{2}-1)}$, given by

$$\mathbf{s}_p = \Theta \mathbf{s}, \tag{12}$$

are placed into $\mathbf{x} \in \mathbb{C}^N$ as

$$\mathbf{x} = \left[0, \mathbf{s}_p^T, 0, \left(\mathbf{K}\mathbf{s}_p^* \right)^T \right]^T, \tag{13}$$

where $\Theta \in \mathbb{R}^{(\frac{N}{2}-1) \times (\frac{N}{2}-1)}$ is DCT pre-coding matrix and $\mathbf{K} \in \mathbb{R}^{(\frac{N}{2}-1) \times (\frac{N}{2}-1)}$ is an exchange matrix such that the elements
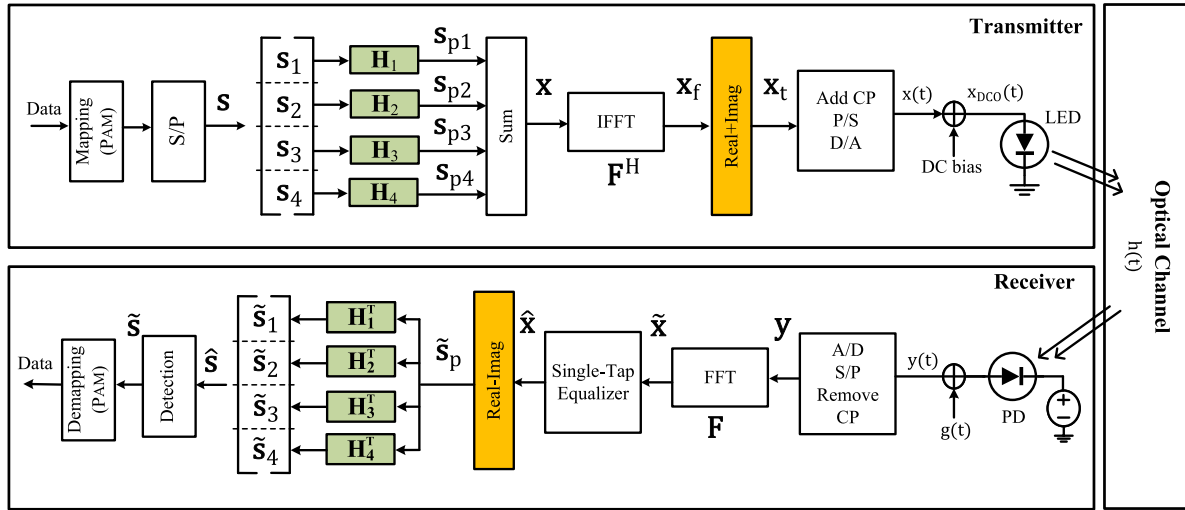
FIGURE 2. Proposed QCTP method for DCO-OFDM.

on the anti-diagonal are 1 and the others are 0. After IFFT implementation, $\mathbf{x}_f = \mathbf{F}^H \mathbf{x}$, it follows the same procedure explained in section II-A.

The inverse pre-coding takes place after equalization on the receiver side by utilizing the inverse DCT matrix, Θ^T, as follows:

$$\tilde{\mathbf{s}} = \Theta^T \tilde{\mathbf{s}}_p. \tag{14}$$

The equalization with the substitution of $\tilde{s}_{p_n}$ in place of $\tilde{s}_n$ as in (9) and the detection after inverse pre-coding are implemented using the same approach outlined in the preceding section.

C. PROPOSED QCTP METHOD FOR DCO-OFDM

The proposed QCTP scheme, as illustrated in Fig. 2, employs four innovative orthogonal QCTP matrices, each with dimensions $N \times \frac{N}{4}$. These matrices are applied to four equally partitioned PAM-modulated symbol subsets, each of size $\frac{N}{4}$, prior to being summed and undergoing the IFFT transformation. Moreover, QCTP incorporates the method from [43] to produce real-valued symbols after IFFT on the transmitter side. Because, when Hermitian symmetry is employed, $\frac{N}{2} - 1$ subcarriers can be used for data transmission in DCO-OFDM, which cannot be divided into four equal parts. In [43], the corresponding real and imaginary components of the complex-valued symbols generated at the output of the IFFT are summed instead of employing Hermitian symmetry at the input of the IFFT. Then these components are subtracted from each other after FFT in the receiver.

In this method, the data are mapped into N real-valued symbols, $\mathbf{s} = [s_0, s_1, \ldots, s_{N-1}]^T \in \mathbb{R}^N$, via a modulation scheme (e.g., PAM), and subsequently these symbols divided into four equal-length arrays; $\mathbf{s}_v \in \mathbb{R}^{\frac{N}{4}}$, where $v = 1, 2, 3, 4$. Each of them is pre-coded by the corresponding QCTP matrix as explained in detail in the following.

The QCTP matrices involved in this scheme utilize the DCT matrix, Θ, as given in section (11), along with the DST matrix, $\Phi = (\phi_{k,l})_{0 \le k,l \le N-1}$ where $\phi_{k,l}$ is the $(k,l)^{th}$ element of $\Phi \in \mathbb{R}^{N \times N}$ and given as

$$\phi_{k,l}$$
$$= \begin{cases} \sqrt{\dfrac{1}{N}}, & k = N - 1 \\ \sqrt{\dfrac{1}{N}} \sin\left[\dfrac{\pi(2l+1)(k+1)}{2N}\right], & k = 0, \ldots, N - 2. \end{cases} \tag{15}$$

The QCTP matrices, $\mathbf{H}_v \in \mathbb{R}^{N \times \frac{N}{4}}$, are given by

$$\mathbf{H}_v = \Gamma_v \mathbf{E}_{\Omega_v}, \tag{16}$$

where $\Gamma_v \in \mathbb{R}^{N \times \frac{N}{4}}$ as given in (17), $\mathbf{E}_{\Omega_v} \in \mathbb{R}^{\frac{N}{4} \times \frac{N}{4}}$ represents eigenvalues of $\Omega_v \in \mathbb{R}^{\frac{N}{4} \times \frac{N}{4}}$ as in (18) and $v = 1, 2, 3, 4$. The matrix notation of obtaining QCTP matrices in (16) is given as follows:

$$\Gamma_1 = [\Theta, \mathbf{K}\Theta, \Theta, \mathbf{K}\Theta]^T \tag{17a}$$
$$\Gamma_2 = [\Phi, -\mathbf{K}\Phi, \Phi, -\mathbf{K}\Phi]^T \tag{17b}$$
$$\Gamma_3 = [\Theta, \mathbf{K}\Theta, -\Theta, -\mathbf{K}\Theta]^T \tag{17c}$$
$$\Gamma_4 = [\Phi, -\mathbf{K}\Phi, -\Phi, \mathbf{K}\Phi]^T \tag{17d}$$

and

$$\Omega_v = \Gamma_v^T \mathbf{C}_r \mathbf{C}_r^T \Gamma_v, \tag{18}$$

where the $\Theta \in \mathbb{R}^{\frac{N}{4} \times \frac{N}{4}}$, $\Phi \in \mathbb{R}^{\frac{N}{4} \times \frac{N}{4}}$, $\mathbf{K} \in \mathbb{R}^{\frac{N}{4} \times \frac{N}{4}}$, and $\mathbf{C}_r \in \mathbb{C}^{N \times N}$ denotes circulant matrix of random typical indoor VLC channel defined in the next section. Note that $\mathbf{C}_r$ is solely utilized for deriving the new pre-coding matrices and remains independent of $\mathbf{C} \in \mathbb{C}^{N \times N}$. After obtaining the QCT pre-coded arrays, $\mathbf{s}_{p_v} \in \mathbb{R}^N$;

$$\mathbf{s}_{p_v} = \mathbf{H}_v \mathbf{s}_v, \tag{19}$$

they are summed as $\mathbf{x} = \sum_{\nu=1}^{4} \mathbf{s}_{p_\nu}$, and then the IFFT is applied (i.e. $\mathbf{x}_f = \mathbf{F}^H \mathbf{x}$). The complex output of the IFFT, $\mathbf{x}_f \in \mathbb{C}^N$, is converted to a real number in this model by adding the real and imaginary values of each symbol, i.e.,

$$\mathbf{x}_t = real(\mathbf{x}_f) + imag(\mathbf{x}_f). \tag{20}$$

In receiver side, $\mathbf{y}$ is calculated as in (6) by replacing $\mathbf{x}_f$ with $\mathbf{x}_t \in \mathbb{R}^N$ and then $\tilde{\mathbf{x}}$ can be estimated as in (7). After the equalization process to obtain $\hat{x}_m$;

$$\hat{x}_m = \frac{\tilde{x}_m}{\Lambda_{m,m}}, \tag{21}$$

where $m = 0, 1, 2, \ldots, N - 1$, the imaginary part of the $\hat{\mathbf{x}}$ is subtracted from the real part of the $\hat{\mathbf{x}}$, i.e.,

$$\tilde{\mathbf{s}}_p = real(\hat{\mathbf{x}}) - imag(\hat{\mathbf{x}}). \tag{22}$$

Then, inverse QCTP matrices are applied to $\tilde{\mathbf{s}}_p \in \mathbb{R}^N$ to obtain respective elements of estimated data arrays, $\tilde{\mathbf{s}}_\nu \in \mathbb{R}^{\frac{N}{4}}$;

$$\tilde{\mathbf{s}}_\nu = \mathbf{H}_\nu^T \tilde{\mathbf{s}}_p, \tag{23}$$

where $\nu = 1, 2, 3, 4$. Following the detection process, the data is acquired through demapping.

III. NUMERICAL RESULTS

The model room, depicted in the top view in Fig. 3 and illuminated by three LED luminaires containing multiple LED chips, is used for CIR calculations. The parameters are outlined in Table 1 and employed in our MATLAB simulations. Furthermore, it is assumed that LEDs adhere to Lambertian radiation patterns (i.e., the semi-angle at half power of the LED = 60°), while reflecting surfaces are modeled as Lambertian reflectors for the sake of simplification.
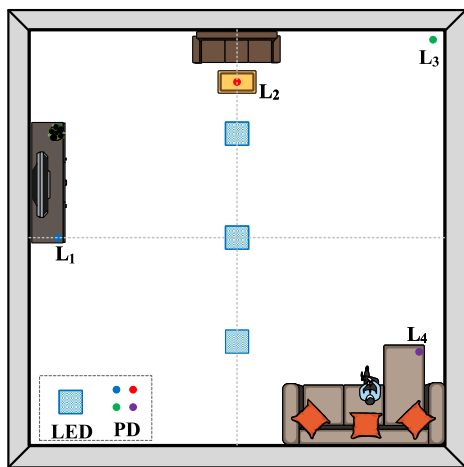

FIGURE 3. Top view of model room.

The CIRs at various locations (L_1, L_2, L_3, L_4) are determined using the ray tracing method detailed in [45], considering the line of sight (LOS) and two reflections (NLOS), as shown in Fig. 4. At L_1, directly aligned

TABLE 1. Model room and simulation parameters.

Parameter	Value
Size of Model Room	$6 \times 6 \times 3$ m
Coordinates of the LED Armatures	$(3, 1.5, 3)$ m $(3, 3, 3)$ m $(3, 4.5, 3)$ m
Direction of the LED Armatures	Elevation: $-90°$ Azimuth: $0°$
Number of LED Chips in the LED Armatures	10×10
LED Chip Model	LXHL-LW6C
LED Chip Power	0.452 W
LED Chip Semi-angle at Half Power	$60°$
Coordinates of PDs	L_1 $(0.5, 3, 0.85)$ m L_2 $(3, 5.25, 1.5)$ m L_3 $(5.75, 5.75, 0)$ m L_4 $(5.5, 1.5, 0.5)$ m
Direction of the PDs	Elevation: $90°$ Azimuth: $0°$
PD Field of View	$85°$
Physical Area of PDs	10^{-4} m^2
Reflection Coefficients	Plaster Side Walls: 0.83 Ceiling: 0.4 Floor: 0.63
Resolution of the Walls for CIR Calculation	25 cm $\times$ 25 cm
Number of Carriers (N)	512
Modulation Level (M)	16
Compression Factor (μ)	3
Number of Attempted Gaussian Matrices (α)	6
DC-Bias	7 dB

horizontally with the center of the three LED lights, the LOS component from the central LED armature is received first, followed by the simultaneous arrival of the LOS components from the edge LED armatures, which dominate the CIR. The NLOS contributions from all LEDs are discernible with exhibiting delays. At L_2, positioned directly in line vertically with all the LED lights, the LOS component from the nearest edge LEDs predominates the CIR. The LOS components from the other LEDs are received with delays corresponding to their respective distances. In this scenario, the strong LOS component overshadows the NLOS contributions, rendering them negligible. At location L_3, in the upper-right corner of the room, the PD is positioned in close proximity to the walls, making the NLOS contributions are prominent and appear sequentially among the received LOS components. At location L_4, similar to L_2, the LOS components are received with delays proportional to their distances, and the NLOS contributions affect the LOS component from the farthest LED armature. The findings demonstrate that the receiver's position, including its height and distance from the LED sources and walls, significantly influences the CIR characteristics. At locations L_1, L_3, and L_4, a frequency-selective multi-tap channel can be experienced when the sampling rate is less than 5 ns. It can be presumed that the typical indoor channel has a strong LOS component (i.e h_0, contains $70 - 85\%$ of received power) and weak NLOS components (i.e h_1, contains $15 - 25\%$ of received power and h_2, contains $5 - 10\%$ of received power) based on our simulations and [45], [46]. Based on this, the utilization of the
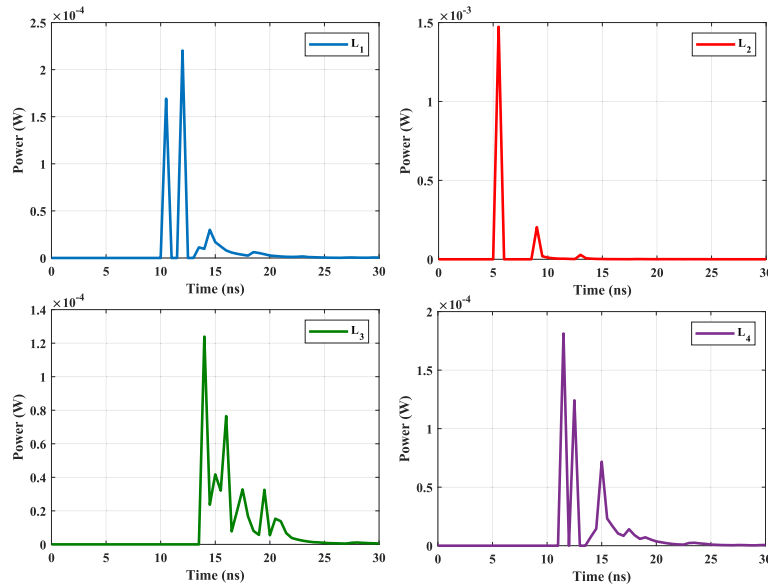
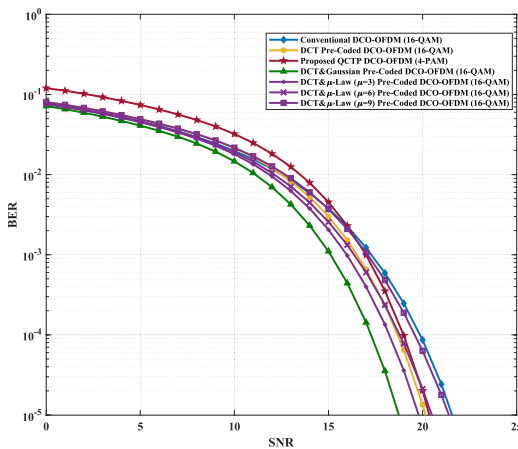**FIGURE 4. Channel impulse response at different receiver positions.**

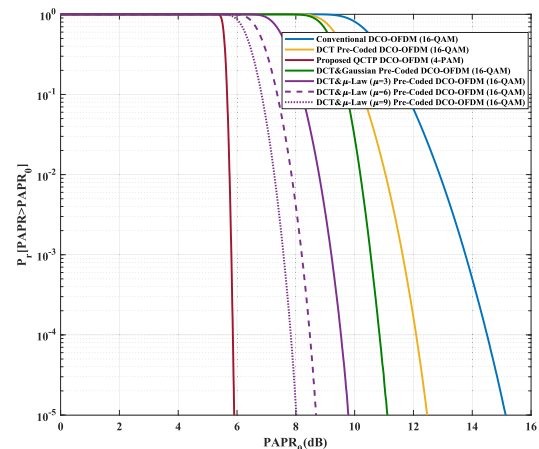**FIGURE 5. Comparative BER performance of the different methods.**

FIGURE 6. Comparative PAPR performance of the different methods.

randomly generated matrix $\mathbf{C_r}$ is employed in the derivation of QCTP matrices.

This study offers a comparative evaluation of BER, PAPR, and computational complexity between DCT pre-coded DCO-OFDM and three distinct pre-coding methodologies hybridized with DCT, specifically DCT with Gaussian matrix [40], DCT with μ-compounding [42], and the proposed QCTP approach. In simulations, the PD, strategically positioned at L_4—distinguished by a frequency-selective CIR shaping circular channel matrix $\mathbf{C}$—is used to evaluate all methods, except for DCT with Gaussian matrix due to its flat single-tap channel constraint. Moreover, it is assumed that the uniform application of the same DC-bias level (i.e. 7 dB for 16-QAM [4]) across all methods ensures the prevention of clipping after DC-bias.

To evaluate the PAPR performance of the methods, the distribution of PAPR, commonly expressed through the

complementary cumulative distribution function (CCDF) as defined in [44], is utilized. M-QAM modulated methods are compared with the proposed $\sqrt{M}$-PAM method to ensure consistent spectral efficiency across all methods. As displayed in Fig. 5, the BER performances of the methods are closely aligned, notwithstanding DCT with Gaussian matrix. Nevertheless, as depicted in Fig. 6, the QCTP exhibits superior PAPR performance, with a reduction exceeding 6 dB relative to the DCT pre-coded method, while DCT with Gaussian matrix (i.e. $\alpha = 6$) [40] and DCT with μ-compounding (i.e. $\mu = 3$) [42] offer reductions of about 1 dB and 2 dB, respectively. Note that increasing the value of μ for PAPR reduction (i.e. $\mu = 6$ or $\mu = 9$) compromises BER performance, highlighting a trade-off between PAPR reduction and BER maintenance.

The simulations are conducted on over 17×10^6 OFDM blocks to ensure robust results and the obtained PAPR values
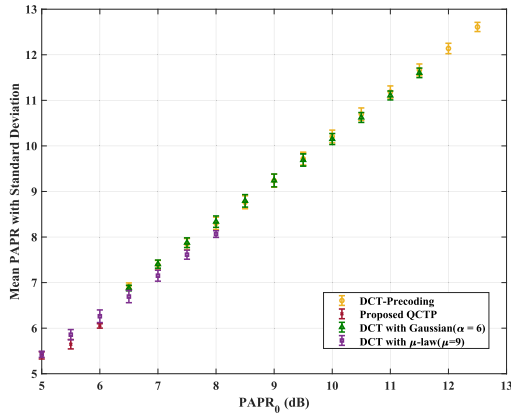
FIGURE 7. Comparative error PAPR bars of the pre-coding methods.

TABLE 2. Matrix multiplication based complexity comparison.

Methods	Transform Marix & Input Vector	Multiplications	Additions
DCT-Precoding	$\boldsymbol{\Theta} \in \mathbb{R}^{(\frac{N}{2}-1)\times(\frac{N}{2}-1)}$ & $\mathbf{s} \in \mathbb{C}^{(\frac{N}{2}-1)}$	$2(\frac{N}{2}-1)^2$	$2(\frac{N}{2}-1)(\frac{N}{2}-2)$
	$\mathbf{F}^H \in \mathbb{C}^{N\times N}$ & $\mathbf{x} \in \mathbb{C}^N$	$4N^2$	$2N^2(2N-2)$
Proposed QCTP	$\mathbf{H_1}, \mathbf{H_2}, \mathbf{H_3}, \mathbf{H_4} \in \mathbb{R}^{\frac{N}{4}\times\frac{N}{4}}$ & $\mathbf{s_1}, \mathbf{s_2}, \mathbf{s_3}, \mathbf{s_4} \in \mathbb{R}^{\frac{N}{4}}$	$4(\frac{N}{4})^2$	$4(\frac{N}{4})(\frac{N}{4}-1)$
	$\mathbf{F}^H \in \mathbb{C}^{N\times N}$ & $\mathbf{x} \in \mathbb{R}^N$	$2N^2$	$2N(N-1)$
	Sum $(s_{p1}, s_{p2}, s_{p3}, s_{p4} \in \mathbb{R}^N)$ and Real+Imag $(x_f \in \mathbb{C}^N)$	−	$3N$ and N
DCT with Gaussian [40]	$\boldsymbol{\Theta} \in \mathbb{R}^{(\frac{N}{2}-1)\times(\frac{N}{2}-1)}$ & $\mathbf{s} \in \mathbb{C}^{(\frac{N}{2}-1)}$	$2(\frac{N}{2}-1)^2$	$2(\frac{N}{2}-1)(\frac{N}{2}-2)$
	$\mathbf{F}^H \in \mathbb{C}^{N\times N}$ & $\mathbf{x} \in \mathbb{C}^N$	$4N^2$	$2N^2(2N-2)$
	$\alpha \times \boldsymbol{\Psi} \in \mathbb{R}^{N\times N}$ & $\mathbf{x_f} \in \mathbb{R}^N$	αN^2	$\alpha N(N-1)$
DCT with μ-law [42]	$\boldsymbol{\Theta} \in \mathbb{R}^{(\frac{N}{2}-1)\times(\frac{N}{2}-1)}$ & $\mathbf{s} \in \mathbb{C}^{(\frac{N}{2}-1)}$	$2(\frac{N}{2}-1)^2$	$2(\frac{N}{2}-1)(\frac{N}{2}-2)$
	$\mathbf{F}^H \in \mathbb{C}^{N\times N}$ & $\mathbf{x} \in \mathbb{C}^N$	$4N^2$	$2N^2(2N-2)$

are counted in bins ranging from 5 dB to 14 dB with 0.5 dB intervals. The mean and standard deviation of each group of bins (e.g., between 5 dB and 5.5 dB) are then calculated and plotted as error bars in Fig. 7. The highest standard deviation observed in our analysis of PAPR is 0.1421. It can also be seen that the QCTP has only three mean PAPR values between 5 dB and 6 dB, while other pre-coding methods exhibit higher mean values in larger ranges.

Table 2 highlights the computational efficiency of the QCTP, performing $\frac{9N^2}{4}$ real multiplications and $\frac{9N^2}{4} + N$ real additions, in contrast to DCT pre-coding which necessitates $\frac{9N^2}{2} - 2N + 2$ real multiplications and $4N^3 - \frac{7N^2}{2} - 3N + 4$ real additions. The primary reason is the recurring pattern in the pre-coding matrices, specifically the repetition of the first $\frac{N}{4}$ rows, exemplified by $\mathbf{H_1} = [\boldsymbol{\beta_1}, \text{flip}(\boldsymbol{\beta_1}), \boldsymbol{\beta_1}, \text{flip}(\boldsymbol{\beta_1})]^T$, where $\boldsymbol{\beta_1}$ corresponds to the initial $\frac{N}{4}$ rows of $\mathbf{H_1}$. This inherent characteristic, also manifests in $\mathbf{x_1}, \mathbf{x_2}, \mathbf{x_3}$, and $\mathbf{x_4}$, facilitates their comprehensive reconstruction from the initial $\frac{N}{4}$ rows, thus permitting the pre-coding matrices to be expressed as $\mathbf{H_1}, \mathbf{H_2}, \mathbf{H_3}$, and $\mathbf{H_4} \in \mathbb{R}^{\frac{N}{4}\times\frac{N}{4}}$, an aspect beneficial for complexity analysis. Fig.8 illustrates the complexity comparison given in Table 2, with specific sections (64, 128, 256) zoomed in to accurately represent the N values of 64, 128, 256, 512, and 1024. The QCTP method demonstrates lower computational complexity compared to DCT pre-coding and other hybrid approaches. DCT with μ-law marginally surpasses the complexity of DCT pre-coding owing to the
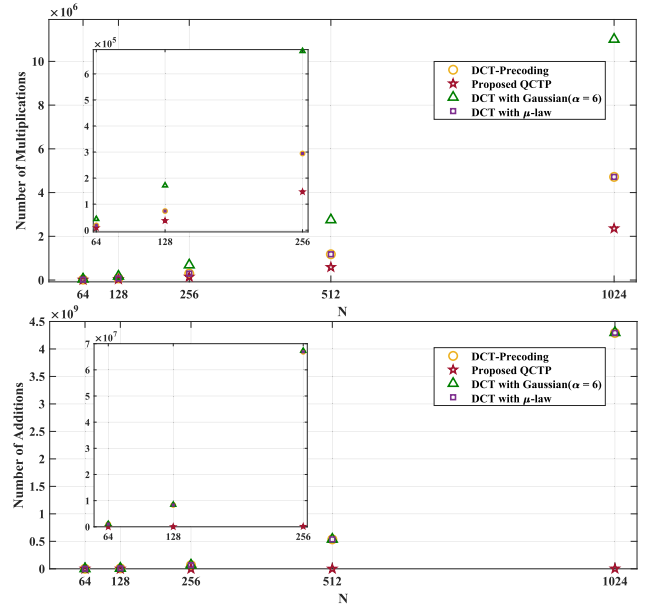

FIGURE 8. Required number of multiplications and additions.

computation of the absolute value of $\mathbf{x}_f$ and its logarithm, as delineated in [42]. Meanwhile, the complexity of DCT with Gaussian [40] escalates proportionally with the number of attempted Gaussian matrices $\boldsymbol{\Psi} \in \mathbb{R}^{N\times N}$, denoted as α, for PAPR minimization. Notably, using fast transform algorithms can potentially reduce DCT with μ-law [42] complexity, rendering it less complex than our proposed method. Nevertheless, the proposed method retains lower complexity than DCT with Gaussian [40].

IV. CONCLUSION

This article proposes a novel pre-coding algorithm, QCTP, for use in IM/DD systems. The QCTP method essentially partitions the modulated data into four equal subsets and then utilizes QCTP matrices prior to the IFFT as a pre-coding scheme. The QCTP approach, similar to other methods, employs a single-tap equalizer for IM/DD systems, which guarantees the preservation of BER performance while substantially enhancing PAPR efficiency. It demonstrates more than 6 dB reduction in PAPR compared to DCT pre-coding and shows superior efficiency compared to other DCT-hybridized (DCT & μ-compounding and DCT & Gaussian) PAPR reduction schemes. Notably, this enhancement is attained with reduced computational demands. In future works, the QCTP matrices could be utilized as transform matrices to enable the transmission of each subset of symbols through distinct light sources, thereby offering the potential for multiple access applications. The QCTP can be applied in experimental settings within RF systems.

REFERENCES

[1] I. Tavakkolnia, D. Cheadle, R. Bian, T. H. Loh, and H. Haas, "High speed millimeter-wave and visible light communication with off-the-shelf components," in *Proc. IEEE Globecom Workshops (GC Wkshps)*, Dec. 2020, pp. 1–6.

[2] Y. Zhou, J. Shi, Z. Wang, J. Zhang, X. Huang, and N. Chi, "Maximization of visible light communication capacity employing quasi-linear preequalization with peak power limitation," *Math. Problems Eng.*, vol. 2016, no. 1, pp. 1–8, 2016.

[3] Z. Ma, X. Li, C. Zhang, L. Turyanska, S. Lin, X. Xi, J. Li, T. Hu, J. Wang, A. Patané, and L. Zhao, "CsPb(Br/I)$_3$ perovskite nanocrystals for hybrid GAN-based high-bandwidth white light-emitting diodes," *ACS Appl. Nano Mater.*, vol. 4, no. 8, pp. 8383–8389, 2021.

[4] S. D. Dissanayake and J. Armstrong, "Comparison of ACO-OFDM, DCO-OFDM and ADO-OFDM in IM/DD systems," *J. Lightw. Technol.*, vol. 31, no. 7, pp. 1063–1072, Apr. 1, 2013.

[5] X. Deng, S. Mardanikorani, G. Zhou, and J. M. G. Linnartz, "DC-bias for optical OFDM in visible light communications," *IEEE Access*, vol. 7, pp. 98319–98330, 2019.

[6] R. Yang, S. Ma, Z. Xu, H. Li, X. Liu, X. Ling, X. Deng, X. Zhang, and S. Li, "Spectral and energy efficiency of DCO-OFDM in visible light communication systems with finite-alphabet inputs," *IEEE Trans. Wireless Commun.*, vol. 21, no. 8, pp. 6018–6032, Aug. 2022.

[7] H. T. Alrakah, T. Z. Gutema, S. Sinanovic, and W. O. Popoola, "PAPR reduction in DCO-OFDM based WDM VLC," *J. Lightw. Technol.*, vol. 40, no. 19, pp. 6359–6365, Oct. 1, 2022.

[8] J. Armstrong and A. J. Lowery, "Power efficient optical OFDM," *Electron. Lett.*, vol. 42, no. 6, p. 370, 2006.

[9] S. Ma, R. Yang, X. Deng, X. Ling, X. Zhang, F. Zhou, S. Li, and D. W. K. Ng, "Spectral and energy efficiency of ACO-OFDM in visible light communication systems," *IEEE Trans. Wireless Commun.*, vol. 21, no. 4, pp. 2147–2161, Apr. 2022.

[10] S. Feng, Q. Wu, C. Dong, and B. Li, "A spectrum enhanced ACO-OFDM scheme for optical wireless communications," *IEEE Commun. Lett.*, vol. 27, no. 2, pp. 581–585, Feb. 2023.

[11] M. Sheikh-Hosseini, M. Hasheminejad, and F. Rahdari, "Linear precoder design for peak-to-average power ratio reduction of generalized frequency division multiplexing signal using gradient descent methods," *Trans. Emerg. Telecommun. Technol.*, vol. 34, no. 2, Feb. 2023, Art. no. e4698.

[12] B. S. D. C. da Silva, V. D. P. Souto, R. D. Souza, and L. L. Mendes, "A survey of PAPR techniques based on machine learning," *Sensors*, vol. 24, no. 6, p. 1918, Mar. 2024.

[13] Y. A. Zenhom, E. K. I. Hamad, M. Alghassab, and M. M. Elnabawy, "Optical-OFDM VLC system: Peak-to-average power ratio enhancement and performance evaluation," *Sensors*, vol. 24, no. 10, p. 2965, May 2024.

[14] M. Laakso, A. A. Dowhuszko, and R. Wichman, "Empirical evaluation of OFDM waveforms for VLC in the presence of LED nonlinearities," in *Proc. IEEE 32nd Annu. Int. Symp. Pers., Indoor Mobile Radio Commun. (PIMRC)*, Sep. 2021, pp. 465–470.

[15] M. Shukla and A. Kumar, "PAPR reduction in OFDM for VLC system," in *Proc. Adv. VLSI, Commun., Signal Process.* Singapore: Springer, 2021, pp. 229–237.

[16] R. Touhami, D. Slimani, A. A. Abdulkafi, Y. S. Hussein, and M. Y. Alias, "Combined envelope scaling with modified SLM method for PAPR reduction in OFDM-based VLC systems," *J. Opt. Commun.*, vol. 44, no. s1, pp. s1175–s1180, Feb. 2024.

[17] Y. Huang, Y. Liu, L. Shi, D. Shi, X. Zhang, E.-H. Aglzim, and J. Zheng, "On improving the accuracy of visible light positioning system with SLM-based PAPR reduction schemes," in *Proc. IEEE Int. Symp. Broadband Multimedia Syst. Broadcast. (BMSB)*, Oct. 2020, pp. 1–5.

[18] J. Tan, Q. Wang, and Z. Wang, "Modified PTS-based PAPR reduction for ACO-OFDM in visible light communications," *Sci. China Inf. Sci.*, vol. 58, no. 12, pp. 1–3, Dec. 2015.

[19] G. Miriyala and V. V. Mani, "A new PAPR reduction technique in DCO-OFDM for visible light communication systems," *Opt. Commun.*, vol. 474, Nov. 2020, Art. no. 126064.

[20] T. Zhang, Z. Tong, W. Zhang, H. Wang, and P. Li, "A novel PAPR reduction scheme based on joint traditional algorithm and machine learning for CO-OFDM systems," *IEEE Photon. Technol. Lett.*, vol. 35, no. 8, pp. 418–421, Apr. 15, 2023.

[21] W. O. Popoola, Z. Ghassemlooy, and B. G. Stewart, "Pilot-assisted PAPR reduction technique for optical OFDM communication systems," *J. Lightw. Technol.*, vol. 32, no. 7, pp. 1374–1382, Apr. 1, 2014.

[22] H. Alrakah, S. Sinanovic, and W. O. Popoola, "Pilot-assisted PAPR reduction in PAM-DMT based visible light communication systems," in *Proc. IEEE Latin-Amer. Conf. Commun. (LATINCOM)*, Nov. 2021, pp. 1–6.

[23] J. Bai, Y. Li, Y. Yi, W. Cheng, and H. Du, "PAPR reduction based on tone reservation scheme for DCO-OFDM indoor visible light communications," *Opt. Exp.*, vol. 25, no. 20, p. 24630, 2017.

[24] M. Rakshit, S. Bhattacharjee, G. Garai, and A. Chakrabarti, "A novel differential evolution algorithm for tone reservation based peak to average power ratio reduction technique in orthogonal frequency division multiplexing systems," *Swarm Evol. Comput.*, vol. 72, Jul. 2022, Art. no. 101086.

[25] B. Wang, Q. Si, and M. Jin, "A novel tone reservation scheme based on deep learning for PAPR reduction in OFDM systems," *IEEE Commun. Lett.*, vol. 24, no. 6, pp. 1271–1274, Jun. 2020.

[26] W. Xu, M. Wu, H. Zhang, X. You, and C. Zhao, "ACO-OFDM-specified recoverable upper clipping with efficient detection for optical wireless communications," *IEEE Photon. J.*, vol. 6, no. 5, pp. 1–17, Oct. 2014.

[27] Z. Wang, P. Wang, X. Nan, S. Niu, S. Chi, H. Che, W. Wang, and W. Pang, "PAPR reduction by combining clipping and piecewise linear companding for OFDM-based VLC systems," *Opt. Eng.*, vol. 60, no. 6, Jun. 2021, Art. no. 066105.

[28] G. Azarnia and A. A. Sharifi, "Clipping-based PAPR reduction of optical OFDM signals using compressive sensing: Bayesian signal reconstruction approach," *Opt. Fiber Technol.*, vol. 64, Jul. 2021, Art. no. 102527.

[29] P. K. Sahoo, Y. K. Prajapati, and R. Tripathi, "Hybrid mapped optical-OFDM using non-linear companding technique for indoor visible light communication application," *IET Commun.*, vol. 14, no. 17, pp. 3073–3079, Oct. 2020.

[30] V. D. Chintala, R. D. Balavendran Joseph, and S. R. Suddapalli, "Joint channel estimation with an enhanced companding PAPR reduction transform for ACO-OFDM system," *Opt. Eng.*, vol. 63, no. 5, May 2024, Art. no. 058104.

[31] J. G. Doblado, A. C. O. Oria, V. Baena-Lecuyer, P. Lopez, and D. Perez-Calderon, "Cubic metric reduction for DCO-OFDM visible light communication systems," *J. Lightw. Technol.*, vol. 33, no. 10, pp. 1971–1978, May 15, 2015.

[32] M. Chen, L. Wang, D. Xi, L. Zhang, H. Zhou, and Q. Chen, "Comparison of different precoding techniques for unbalanced impairments compensation in short-reach DMT transmission systems," *J. Lightw. Technol.*, vol. 38, no. 22, pp. 6202–6213, Nov. 15, 2020.

[33] H. Mathur and T. Deepa, "A novel precoded digitized OFDM based NOMA system for future wireless communication," *Optik*, vol. 259, Jun. 2022, Art. no. 168948.

[34] B. Ranjha and M. Kavehrad, "Precoding techniques for PAPR reduction in asymmetrically clipped OFDM based optical wireless system," *Proc. SPIE*, vol. 8645, pp. 183–191, Jan. 2013.

[35] R. Ahmad and A. Srivastava, "PAPR reduction of OFDM signal through DFT precoding and GMSK pulse shaping in indoor VLC," *IEEE Access*, vol. 8, pp. 122092–122103, 2020.

[36] G. M. Salama, H. F. Abdalla, A. A. Mohamed, E. S. Hassan, M. I. Dessouky, A. A. M. Khalaf, A. El-Emary, and A. S. Elsafrawey, "PAPR reduction technique for FBMC based visible light communication systems," *IET Commun.*, vol. 16, no. 15, pp. 1807–1814, Sep. 2022.

[37] J. Zhou and Y. Qiao, "Low-PAPR asymmetrically clipped optical OFDM for intensity-modulation/direct-detection systems," *IEEE Photon. J.*, vol. 7, no. 3, pp. 1–8, Jun. 2015.

[38] M. K. Mohaisen, M. T. Hamood, and M. S. Ahmed, "Reducing peak to average power ratio (PAPR) for visible light communications (VLC) system using Walsh–Hadamard precoded discrete Hartley transforms," *J. Opt. Commun.*, Nov. 2022. [Online]. Available: https://www.degruyter.com/journal/key/joc/0/0/html and https://www.degruyter.com/document/doi/10.1515/joc-2022-0102/html

[39] N. Li, Y. Zhang, Y. Zhang, and C.-C. J. Kuo, "On energy compaction of 2D Saab image transforms," in *Proc. Asia–Pacific Signal Inf. Process. Assoc. Annu. Summit Conf. (APSIPA ASC)*, Nov. 2019, pp. 466–475.

[40] B. Taha, H. A. Fayed, M. H. Aly, and M. Mahmoud, "A reduced PAPR hybrid OFDM visible light communication system," *Opt. Quantum Electron.*, vol. 54, no. 12, p. 815, Dec. 2022.

[41] Z.-P. Wang and S.-Z. Zhang, "Grouped DCT precoding for PAPR reduction in optical direct detection OFDM systems," *Optoelectron. Lett.*, vol. 9, no. 3, pp. 213–216, May 2013.

[42] M. Y. El-Ganiny, A. A. Khalaf, A. I. Hussein, and H. F. A. Hamed, "Hybrid PAPR reduction schemes for different OFDM-based VLC systems," *Opto-Electron. Rev.*, vol. 30, Aug. 2022, Art. no. e141951.

[43] G. Hacioglu, C. Albayrak, and K. Turk, "Optical OFDM waveform construction by combining complex symbols' component of IFFT," *Phys. Commun.*, vol. 60, Oct. 2023, Art. no. 102137.

[44] I. Cinemre and G. Hacioglu, "A DCT/DST based fast OFDM method in IM/DD systems," *IEEE Commun. Lett.*, vol. 25, no. 9, pp. 3013–3016, Sep. 2021.

[45] K. Lee, H. Park, and J. R. Barry, "Indoor channel characteristics for visible light communications," *IEEE Commun. Lett.*, vol. 15, no. 2, pp. 217–219, Feb. 2011.

[46] M. Uysal, F. Miramirkhani, O. Narmanlioglu, T. Baykas, and E. Panayirci, "IEEE 802.15.7r1 reference channel models for visible light communications," *IEEE Commun. Mag.*, vol. 55, no. 1, pp. 212–217, Jan. 2017.

GOKCE HACIOGLU is currently a Professor with the Department of Electronics Engineering, Karadeniz Technical University. His current research interests include multiple access techniques, routing algorithms of wireless sensor networks (WSN), signal strength-based positioning, visible light, and powerline communications.

TOKTAM MAHMOODI (Senior Member, IEEE) received the B.Sc. degree in electrical engineering from the Sharif University of Technology, Tehran, Iran, in 2002, and the Ph.D. degree in telecommunications from King's College London, London, U.K., in 2009. She was a Visiting Research Scientist with F5 Networks, San Jose, CA, USA, in 2013, a Postdoctoral Research Associate with the ISN Research Group, Electrical and Electronic Engineering Department, Imperial College London, London, from 2010 to 2011, and a Mobile VCE Researcher, from 2006 to 2009. She has also worked in the mobile and personal communications industry, from 2002 to 2006, and in a research and development team on developing DECT standard for WLL applications. She has contributed to and led a number of FP7, H2020, and EPSRC-funded projects, advancing mobile and wireless communication networks. She is currently the Head of the Centre for Telecommunications Research, Department of Engineering, King's College London, where she is a Professor of communication engineering. Her research interests include network intelligence, and mission-critical networking with impact in healthcare, automotive, and smart cities.
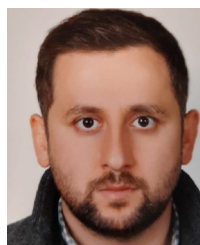
IDRIS CINEMRE (Member, IEEE) received the M.Sc. degree (Hons.) in mobile and personal communications from the King's College London, in 2013, and the Ph.D. degree in telecommunications from Karadeniz Technical University, in 2024. Currently, he is pursuing the second Ph.D. degree in telecommunications with a specialization in conflict resolution within intent-driven networks and open RAN. From 2014 and 2021, he was a Research Assistant in Türkiye. His doctoral research focused on PAPR reduction techniques and the application of DCT in OFDM structures for VLC. He received the Postgraduate Scholarships from the Ministry of National Education, Türkiye, in 2011 and 2018, supporting his pursuit of both the M.Sc. and Ph.D. degrees in U.K.

• • •